

Cite this: *Mater. Adv.*, 2024,  
5, 8534

# Thiourea-based rotaxanes: anion transport across synthetic lipid bilayers and antibacterial activity against *Staphylococcus aureus*<sup>†</sup>

Nasim Akhtar,<sup>‡a</sup> Udyogi N. K. Conthagamage,<sup>‡a</sup> Sara P. Bucher,<sup>b</sup>  
Zuliah A. Abdulsalam,<sup>a</sup> Macallister L. Davis,<sup>a</sup> William N. Beavers<sup>id</sup>\*<sup>b</sup> and  
Víctor García-López<sup>id</sup>\*<sup>a</sup>

We report the synthesis of two rotaxanes (**1** and **2**) whose rings have appended thiourea units for the selective recognition of Cl<sup>−</sup> anions. Rotaxane **1** transports Cl<sup>−</sup> across synthetic lipid bilayers more efficiently than **2**, exhibiting EC<sub>50</sub> values of 0.243 mol% versus 0.736 mol%, respectively. A control rotaxane (**3**) without the thiourea units and the individual axle (**4**) also showed Cl<sup>−</sup> transport, although with much lower efficiency (EC<sub>50</sub> values of 4.044 mol% and 4.986 mol%). The unthreaded ring (**5**) showed the lowest transport activity. This trend highlights the advantage of the interlocked system with a ring containing thiourea units. We also investigated how the membrane composition of liposomes influences the transport activity of **1** and **2**, observing higher Cl<sup>−</sup> transport in membranes with higher fluidity. Additionally, we demonstrated that rotaxane **1** can kill drug-resistant and osmotolerant *Staphylococcus aureus* when used in combination with NaCl or arachidonic acid. The latter is known to increase the fluidity of the membrane in *S. aureus*, highlighting cooperative behavior. This work provides new insights into how various structural features and the membrane environment influence the anion transport activity of rotaxanes, offering important design principles for optimizing future rotaxanes for biomedical and other applications.

Received 6th August 2024,  
Accepted 29th September 2024

DOI: 10.1039/d4ma00794h

rsc.li/materials-advances

## 1. Introduction

Synthetic molecular transporters that facilitate the movement of ions across membranes are significant for many applications, such as biosensors, nanofluidic devices, nanofiltration, water purification, and energy storage and conversion.<sup>1–7</sup> Synthetic transporters are also useful in medicine to treat channelopathies caused by defective protein ion transporters.<sup>1,8,9</sup> They have also been used to dysregulate ion balance and kill cancer cells and bacteria.<sup>10–19</sup>

Our team is exploring new approaches to fight antibiotic-resistant bacteria, such as *Staphylococcus aureus*, in response to the escalating health crisis caused by the declining efficacy of traditional antibiotics.<sup>20,21</sup> *S. aureus* is a major human pathogen that can infect every niche of the human host and is increasingly becoming more resistant to antimicrobials.<sup>22,23</sup>

For instance, in 2019, drug-resistant *S. aureus* was associated with nearly one million deaths worldwide.<sup>24</sup> Additionally, *S. aureus* is osmotolerant, needing NaCl concentrations exceeding 2.5 M to inhibit growth completely. This presents a major problem for food manufacturers in preventing contamination during preservation and the resulting cases of food poisoning or lost products.<sup>25</sup> Therefore, there is a need for novel synthetic molecules that can kill *S. aureus*.

Recently, systems based on artificial molecular switches and machines have shown excellent capabilities for ion transport in synthetic lipid bilayers.<sup>26–28</sup> These molecules are much simpler than biological proteins but possess the potential to mimic their functionality while offering adaptability and versatility for use in various environments and applications.<sup>29–32</sup> They utilize a conformational change or the mechanical movement of their sub-molecular components to physically move the ions across the bilayer. Such transport mechanisms differ from the ones used by traditional artificial ion channels and diffusion-based carriers, which have been extensively investigated.<sup>1,33</sup>

One system that has been underexplored is rotaxanes. Bao and coworkers demonstrated that some rotaxanes can transport K<sup>+</sup> cations across lipid bilayers.<sup>34,35</sup> Through molecular dynamic simulations, they proposed that transport occurs due

<sup>a</sup> Department of Chemistry, Louisiana State University, Baton Rouge, LA 70803, USA. E-mail: vglopez@lsu.edu<sup>b</sup> Department of Pathobiological Sciences, Louisiana State University School of Veterinary Medicine, Baton Rouge, LA 70803, USA. E-mail: wbeavers@lsu.edu<sup>†</sup> Electronic supplementary information (ESI) available. See DOI: <https://doi.org/10.1039/d4ma00794h><sup>‡</sup> Equal contribution.

to the shuttling movement of the ring carrying the cations along a transmembrane axle.<sup>36</sup> By incorporating triazole derivatives at both ends of the axle, a similar rotaxane also transports  $\text{Cl}^-$  anions; however, in this design, the anions are transported solely through a relay mechanism rather than by the shuttling of the ring carrying the ion.<sup>37,38</sup>

Rotaxane-based transporters are still in their infancy, and their operation needs to be optimized and fully understood. For instance, elucidating how rotaxanes work across different lipid membranes has remained elusive as previous systems were investigated in membranes of a single composition. Addressing this knowledge gap is essential to designing more efficient rotaxanes for future applications. For example, it is known that changes in fluidity in biological membranes directly impact the function of transport proteins and will likely affect synthetic transporters, too.<sup>39,40</sup> Lastly, to the best of our knowledge, there are no examples of rotaxanes with ion transport capability being studied as antibacterial agents.

Therefore, the goals of this study were to design rotaxanes with previously unexplored structural features to transport  $\text{Cl}^-$  anions across synthetic lipid bilayers and to investigate how lipid membranes of different fluidity impact their transport activity. Additionally, we conducted an initial assessment of the potential of these rotaxanes to kill *S. aureus*. Accordingly, we synthesized two rotaxanes with anion recognition units, specifically thiourea groups, appended on the ring rather than in the axle to bind and transport  $\text{Cl}^-$  anions (Fig. 1).

Through various assays, we confirmed the ability of our thiourea-based rotaxanes to transport  $\text{Cl}^-$  anions selectively

without disrupting the membrane in liposomes and established the influence of membrane fluidity. Remarkably, when tested in *S. aureus*, rotaxane **1** inhibited bacterial growth in the presence of NaCl (1 M) in the media. Additionally, rotaxane **1** effectively killed *S. aureus* at an even lower NaCl (85 mM) concentration when arachidonic acid (AA) was added, which is known to increase the membrane fluidity of *S. aureus*.<sup>21,41</sup>

Our findings provide important insights into the operation of rotaxanes within lipid membranes, emphasizing the need to consider both molecular structure and the surrounding environment in their design and operation. Furthermore, the demonstrated antibacterial activity of rotaxane **1** underscores the potential for developing new rotaxane-based antibacterial agents. This encourages further exploration and future mechanistic investigations to gain deeper insights into their bactericidal mechanisms.

## 2. Result and discussion

### 2.1 Molecular design

We designed three unique rotaxanes (**1–3**) with variations in their axle or ring functionalization (Fig. 1). Specifically, rotaxane **1** features a macrocyclic ring constructed from a dibenzo-24-crown-8 framework armed with two thiourea units for the selective recognition of  $\text{Cl}^-$  anions. The inclusion of electron-withdrawing trifluoromethyl ( $-\text{CF}_3$ ) groups serves a dual purpose: first, to increase the acidity of the  $-\text{NH}$  groups, thereby

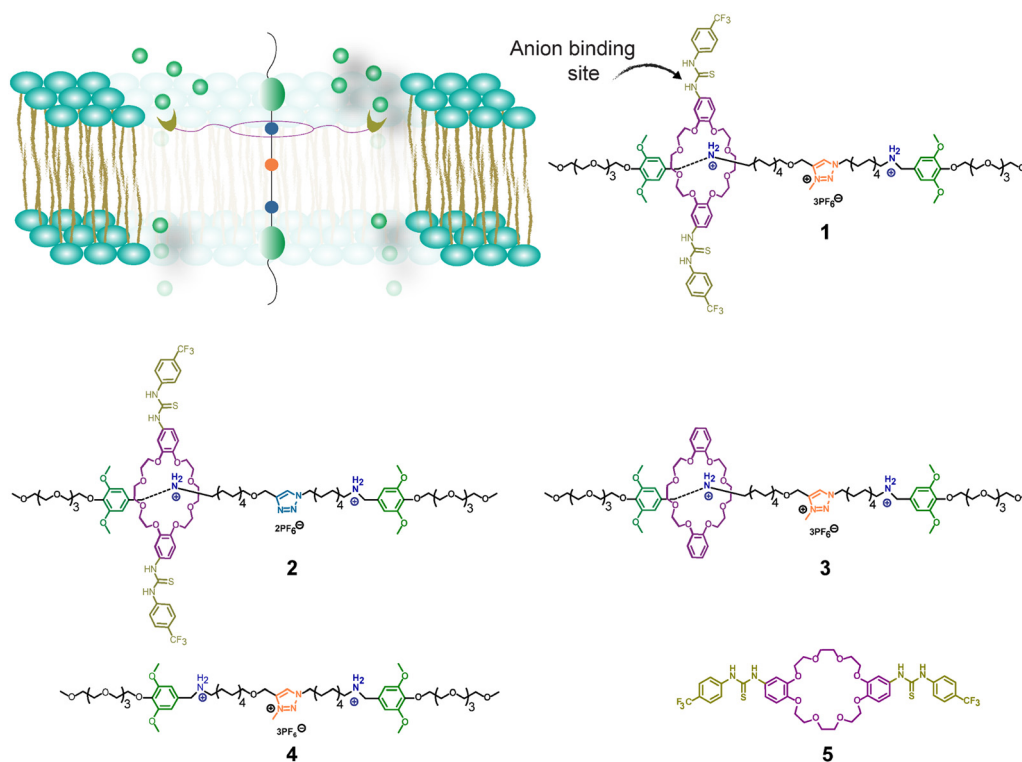


Fig. 1 Representation of a thiourea-based rotaxane operating in lipid membranes and structures of rotaxanes **1**, **2** and control molecules **3**, **4**, and **5**. BAA stations are in dark blue, and MTA stations are in orange.



intensifying the affinity for the anions, and secondly, to enhance the ring's hydrophobicity, facilitating its operation within the lipid bilayer. As a result of these modifications, the estimated  $\log P$  value for the utilized ring stands at 8.61, notably higher than for the ring without  $-\text{CF}_3$  groups ( $\log P = 6.86$ , calculated by MarvinSketch 17.27 program).

We employed an axle previously used by Bao and colleagues. It contains tetraethylene glycol (PEG) chains at each extreme as the hydrophilic units interacting with the polar heads of the lipids.<sup>34</sup> *O*-Dimethoxy benzene groups located between the PEGs and an amphiphilic spacer are used as the stoppers to avoid the dethreading of the rings. The spacer comprises an aliphatic chain housing two benzyl alkylammonium hexafluorophosphate (BAA) stations and an *N*-methyl triazolium hexafluorophosphate (MTA) station in the middle (Fig. 1).

The thermodynamic trapping of the ring within the BAA stations is attributed to their strong non-covalent interactions, enabling the ring to stochastically shuttle between these two BAA stations. Moreover, the MTA unit acts as a weaker recognition site, reducing the energy barrier for shuttling. Consequently, the MTA unit expedites the movement of the ring by serving as a central relay (Fig. S12a and b, ESI†).<sup>42–44</sup> Accordingly, rotaxane 2, equipped with a non-methylated triazole unit (light blue, Fig. 1), exhibits slower shuttling than 1 and 3. On the other hand, rotaxane 3 uses the same axle as 1 but lacks the thiourea units on the ring, serving as a control in our study to assess the role of these groups in facilitating anion transportation.

Additionally, we studied the individual axle 4 as a control molecule to determine the potential role of the ammonium units in anion transport. Ring 5 serves to assess the binding affinity for the anions and to determine if it can transport anions when it is not threaded to the axle.

## 2.2 Synthesis of target molecules

The target rotaxanes (Fig. 1) were synthesized through the dumbbell capture strategy.<sup>45</sup> Thus, we first separately synthesized the boc-protected ring 6 and the axle fragments 7 and 8 with a terminal alkyne and an azide group, respectively (Schemes S1–S4, ESI†).<sup>34,46,47</sup> It is important to note that ring 6 was obtained as a mixture of *syn* and *anti*-constitutional isomers, which could not be separated, but only the *syn* isomer is drawn here for simplicity.<sup>46,47</sup> However, we believe this might not significantly impact the transport, as the rings are flexible.

Furthermore, as shown in Scheme 1, the threading of ring 6 onto axle fragment 7 forms a pseudorotaxane. Then, a copper(i)-catalyzed azide–alkyne cycloaddition (CuAAC) reaction between this pseudorotaxane and 8 gives rotaxane 9 in 22% yield.

To obtain rotaxane 1, we methylated the triazole ring and then removed the Boc protecting groups in the rings. Lastly, the diamino ring reacted with 4-(trifluoromethyl)phenyl isothiocyanate to generate the final rotaxane 1 in a 36% yield.

Rotaxane 2 was synthesized similarly to 1 but without the methylation step. On the other hand, control rotaxane 3 was prepared similarly to 1 but using the unfunctionalized dibenzo-24-crown-8 ring 10 instead (Scheme S9, ESI†). Axle 4 was obtained after the CuAAC click reaction between 7 and 8 (Scheme S10, ESI†).

We also synthesized ring 5 for NMR binding studies (Scheme S1, ESI†). It is important to mention that rotaxane 1 could not be synthesized by threading thiourea-functionalized ring 5 directly onto any of the axle fragments due to its low solubility in moderately polar solvents like dichloromethane. Moreover, using more polar solvents like DMF and DMSO did not work due to their propensity to form competitive hydrogen bonds with the ring, suppressing the threading process (Scheme S5, ESI†).<sup>48</sup> Therefore, we designed the synthetic route described in Scheme 1.

## 2.3 Anion recognition in solution

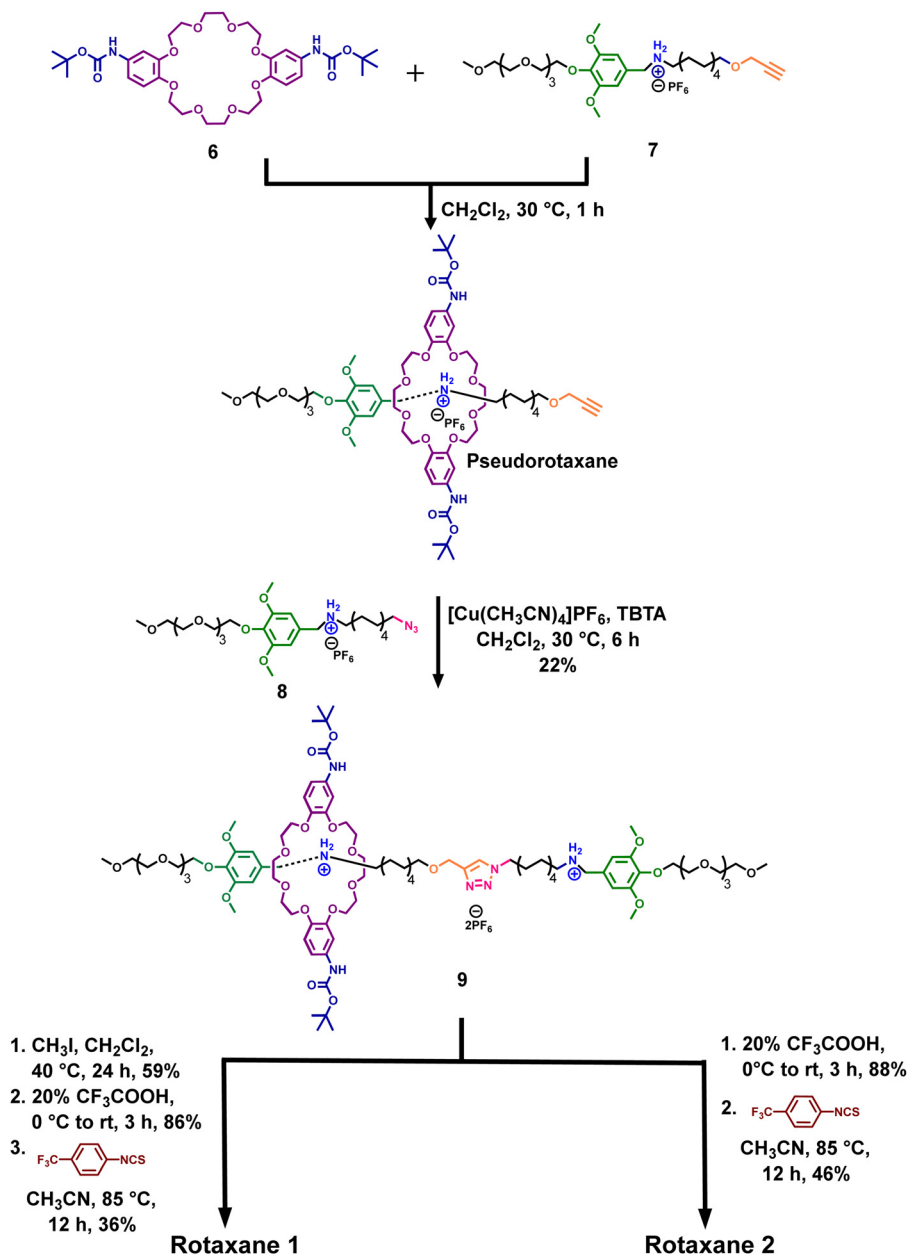
The efficiency of the thiourea moieties in the newly designed ring 5 to bind  $\text{Cl}^-$  anions was evaluated by  $^1\text{H}$  NMR titrations in acetonitrile- $\text{d}_3$ . A fixed amount of 5 (5 mM) was used against different concentrations of tetrabutylammonium chloride ( $[\text{TBACl}] = 0\text{--}100\text{ mM}$ ) as the source of  $\text{Cl}^-$  anions. Upon successive addition of TBACl, the N–H chemical shifts of the thiourea moved downfield, indicating the anion binding (Fig. 2 and Fig. S1, ESI†). The corresponding binding constant ( $K_a$ ) was determined to be  $198.5 \pm 8.0\text{ M}^{-1}$  when fitting the data to a 1 : 1 binding model using the BindFit v0.5 program.<sup>49,50</sup> Similar  $^1\text{H}$  NMR titrations with TBABr, TBAl, and  $\text{TBANO}_3$  were done to determine the  $K_a$  for the corresponding anions (Fig. S2–S7, ESI†). Remarkably, ring 5 exhibits higher selectivity for  $\text{Cl}^-$  anions, displaying a preference in the following order:  $\text{Cl}^- > \text{Br}^- > \text{NO}_3^- > \text{I}^-$  (Table 1). Furthermore, mass spectrometric analysis indicated the formation of the  $[\text{5-Cl}]^-$  complex (Fig. S10, ESI†). However, when the data was fitted to a non-cooperative 1 : 2 binding model, the  $K_a$  for  $\text{Cl}^-$  was estimated at  $1204.9 \pm 273.5\text{ M}^{-1}$ , but no good fitting was obtained for any of the other anions under this model. This suggests an intriguing binding of the anions in the free ring (Fig. S8 and Table S2, ESI†), which could be due to the flexibility of the ring to adopt a geometry favoring the binding of chloride.

## 2.4 Shuttling of rotaxanes in solution

An important feature of the rotaxanes is the shuttling of the ring along the axle. Therefore, we used two-dimensional exchange spectroscopy (2D-EXSY) to measure the shuttling rate ( $k$ ) of four rotaxanes differing in the axle or the ring functionalization. Specifically, we studied rotaxane 3 and 20, both featuring the MTA station in the axle but differing in the functionalization of the ring. Rotaxane 20 has a ring functionalized with two boc-protected amines (Fig. S11, ESI†). Similarly, we studied their non-methylated counterparts, rotaxanes 23 and 9 (Fig. S11, ESI†). We focused on these rotaxanes because determining the shuttling rate of 1 by NMR proved challenging due to signal overlap among the protons used to monitor the motion.

We measured shuttling rates ( $k$ ) of 0.087 Hz and 0.056 Hz for rotaxanes 3 and 20, respectively, confirming the shuttling motion of the ring along the axle when investigated in acetonitrile- $\text{d}_3$  (Fig. S12–S17 and Tables S3 and S4, ESI†). This is in agreement with Bao's work, where a different ring shuttles along the same axle at 0.082 Hz in a 1 : 1 mixture of chloroform- $\text{d}$  and acetonitrile- $\text{d}_3$ . These findings indicate that, to some extent, dibenzo-24-crown-8



Scheme 1 Synthesis of rotaxanes **1** and **2**.

rings exhibit similar shuttle rates in solution regardless of the specific moieties attached. Therefore, it is reasonable to infer that rotaxane **1** would exhibit similar shuttling motion as the thiourea units are not much larger than the other moieties investigated. On the other hand, we did not observe shuttling motion for any of the non-methylated rotaxanes (**9** and **23**) during the same time scale of the experiments used in the other systems, indicating that shuttling is much slower than in their counterparts with the MTA station in the axle. Therefore, rotaxane **2** should exhibit minimal shuttling compared to **1**.

## 2.5 Selective transport of $\text{Cl}^-$ anions across synthetic lipid bilayers

We investigated the ability of rotaxanes **1–3**, axle **4**, and ring **5** to transport  $\text{Cl}^-$  anions across the lipid bilayers of large

unilamellar vesicles (LUVs) composed of egg yolk phosphatidylcholine (EYPC) and cholesterol (Chol) in an 8 : 2 molar ratio. Inside the vesicle, the medium contained 5 mM phosphate buffer at pH 7.2 and 100 mM NaCl, while the external medium contained 5 mM phosphate buffer at pH 7.2 and 100 mM  $\text{NaNO}_3$ .<sup>13,51</sup> We monitored the efflux of  $\text{Cl}^-$  anions over time using a chloride ion-selective electrode (ISE). The monitoring started after adding the compounds dissolved in dimethyl sulfoxide (DMSO) at 50 seconds and without applying any pH gradient (Fig. 3a). At 600 seconds, Triton X-100 was added to lyse the vesicle (Fig. 3b).

We observed a constant increment in the external  $\text{Cl}^-$  anion concentration over time after adding rotaxane **1**, demonstrating the transport activity of our molecule (Fig. 3c). Moreover, by



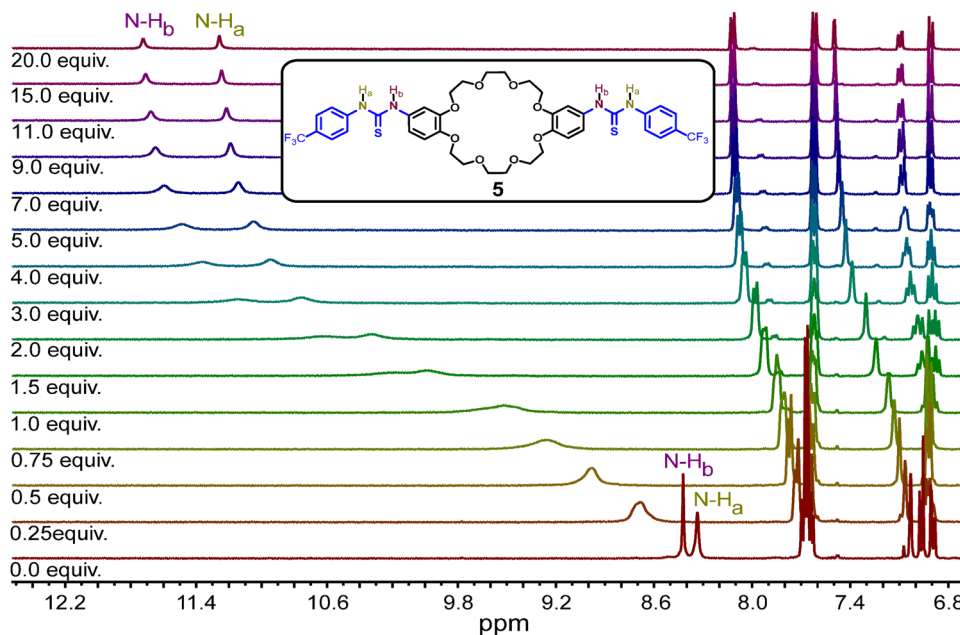


Fig. 2 Recognition and binding of  $\text{Cl}^-$  anions by thiourea units on ring **5**.  $^1\text{H}$  NMR spectra showing the chemical shift of the N–H signals during the titration of ring **5** with different equivalents of TBACl in acetonitrile- $\text{d}_3$ .

investigating the transport of  $\text{Cl}^-$  anions using varying mol% of rotaxane **1** with respect to the lipid content, we established its  $\text{EC}_{50}$  value as 0.243 mol% (Fig. 3d). Rotaxane **2** exhibited an  $\text{EC}_{50}$  value of 0.736 mol%, while rotaxanes **3** and **4** also transported anions across the bilayer but with much lower efficiency. We estimated  $\text{EC}_{50}$  values of 4.044 mol% and 4.986 mol% for **3** and **4**, respectively (Fig. S18, S19 (ESI $^\dagger$ ) and Table 2). Moreover, we observed far inferior transport activity with ring **5** compared to the other molecules, and determining its  $\text{EC}_{50}$  value was not possible due to the necessity of a high amount of ring **5**, which resulted in its precipitation (Fig. S20, ESI $^\dagger$ ).

To better illustrate the difference in transport activity among all the synthesized compounds, we monitored the  $\text{Cl}^-$  anions efflux using **1**–**5** at the same mol% (0.499 mol%) (Fig. 4). The results show the clear superiority of rotaxane **1**, followed by rotaxane **2** and then rotaxane **3**. Moreover, the individual components, axle **4** and ring **5**, show the least transport activity. Adding the same amount of dimethyl sulfoxide (DMSO) without rotaxane did not cause significant  $\text{Cl}^-$  efflux.

These data show the superiority of the interlocked system where the ring has anion recognition units, such as in rotaxanes **1** and **2**. The transport activity shown by **3** and **4** lacking thiourea

units might be attributed to the positive charges in the axle, which could weakly interact with the  $\text{Cl}^-$  anions and facilitate their transport across the bilayer. Thus, it is likely that this relay-type mechanism also contributes at least partially to the transport observed in **1** and **2**. This could explain the transport activity of rotaxane **2**, which, according to our shuttling studies in solution, is not expected to shuttle or should shuttle much slower than rotaxane **1**. Hence, rotaxane **2** was expected to show much lower transport activity if shuttling was the only transport mechanism.

Nevertheless, the higher anion transport activity of rotaxane **1** demonstrates the advantage of incorporating anion recognition units in a ring that could potentially move along the axle. Thus, we can tentatively attribute a combination of shuttling and relay-based transport in rotaxane **1**. However, disentangling the contributions of these possible mechanisms requires a separate study of different rotaxanes of various structural designs. Still, our findings here provide valuable insights into the structural design of rotaxanes for anion transport.

Moreover, we studied rotaxane **1** further to gain insight into its operation in different membranes. First, we investigated if rotaxane **1** selectively transports specific anions. As shown in Fig. 5a and Fig. S21–S23 (ESI $^\dagger$ ), rotaxane **1** shows selective transport of  $\text{Cl}^-$  anions over  $\text{Br}^-$ ,  $\text{I}^-$ , and  $\text{NO}_3^-$  anions when investigated using the corresponding ion selective electrodes. However, such selectivity could originate from different responses from the electrodes. Moreover, the Gale group recently reported that studies using ion-selective electrodes might produce an apparent selectivity for chloride, even when actual selectivity for this anion is absent, so they proposed a fluorescence-based assay to study anion selectivity.<sup>52</sup>

Therefore, we investigated rotaxane **1** using the anion gradient assay (without any base pulse) developed by the Gale

Table 1 Binding constants of **5** for different anions in acetonitrile- $\text{d}_3$

Anion	$K_a^a$ ( $\text{M}^{-1}$ ) from 1 : 1 binding model
$\text{Cl}^-$	$198.5 \pm 8.0$
$\text{Br}^-$	$130.8 \pm 5.0$
$\text{NO}_3^-$	$20.9 \pm 0.1$
$\text{I}^-$	$90.2 \pm 1.0$

<sup>a</sup> Note: this is the average  $K_a$  calculated from three independent titrations for each anion.





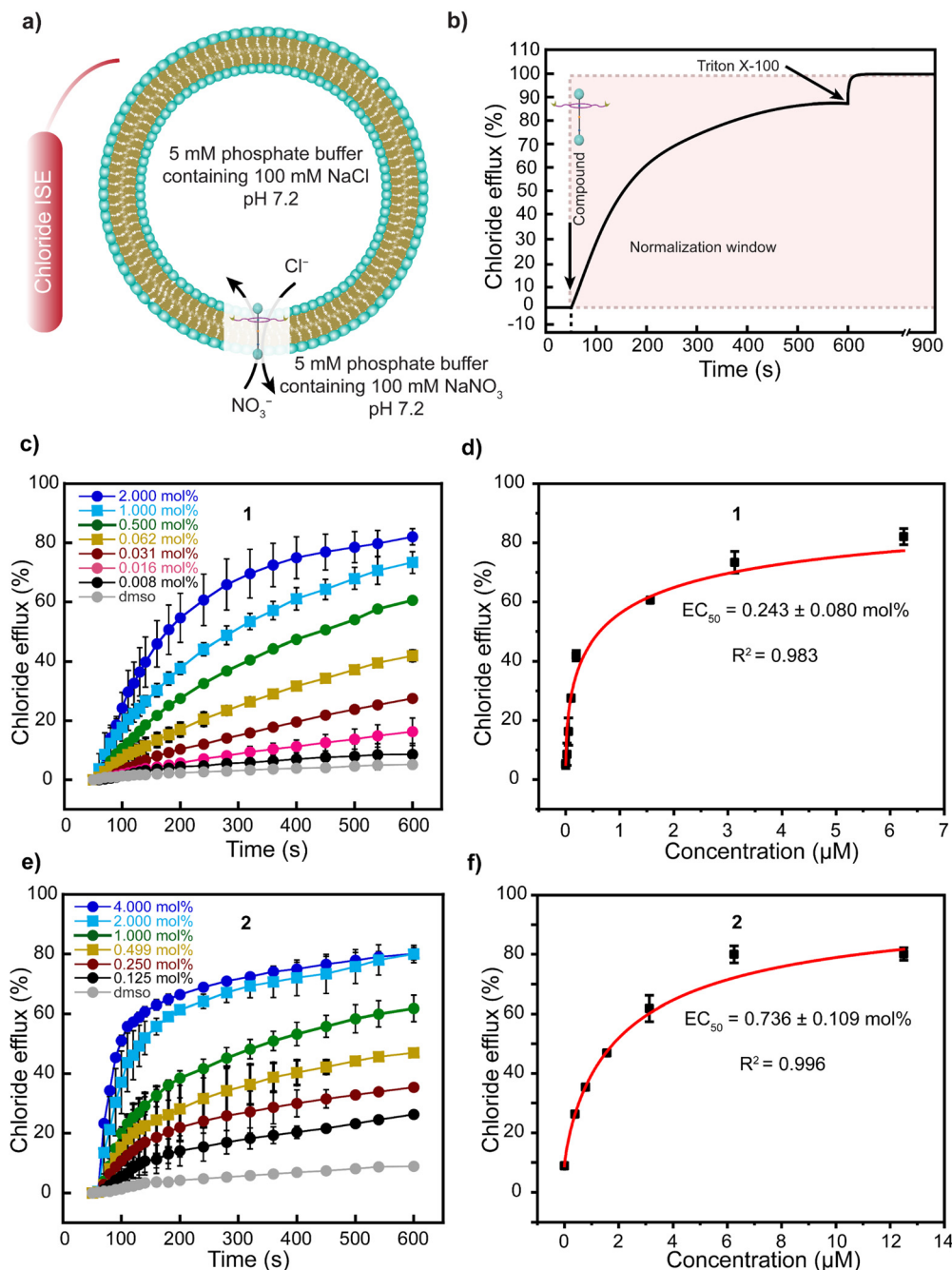


**Fig. 3** Transport of  $\text{Cl}^-$  anions across the bilayer of LUVs (EYPC/Chol, 8 : 2 molar ratio) by rotaxanes **1** and **2**. (a) Representation of anions transport monitored by a chloride selective electrode. (b)  $\text{Cl}^-$  anions efflux kinetics across the LUVs. (c) Transport of  $\text{Cl}^-$  anions over time by different mol% of rotaxane **1**. (d) Fitting curve of hill analysis to determine the  $\text{EC}_{50}$  value for rotaxane **1**. (e) Transport of  $\text{Cl}^-$  anions over time by different mol% of rotaxane **2**. (f) Fitting curve of Hill analysis to determine the  $\text{EC}_{50}$  value for rotaxane **2**. Gray curves correspond to the sample where the DMSO stock solution was added to the LUVs without the rotaxane. Error bars represent standard deviations from two runs. Some error bars, though present, are so small that they are overshadowed by the symbols representing the data points.

group, where the chloride anions are encapsulated inside the vesicle, and  $\text{NaX}$  ( $\text{X} = \text{Br}^-$ ,  $\text{I}^-$ , and  $\text{NO}_3^-$ ) is kept in the outside.<sup>52,53</sup> Our findings reveal  $\Delta\text{pH}_{\text{max}}$  values indicating the selectivity sequence of  $\text{Cl}^- > \text{Br}^- \approx \text{NO}_3^- \approx \text{I}^-$  (Fig. S24–S28, ESI†). This result confirms the selectivity of rotaxane **1** to transport  $\text{Cl}^-$ , which is surprising. Separate studies will be conducted to elucidate the contributions of the interfacial binding

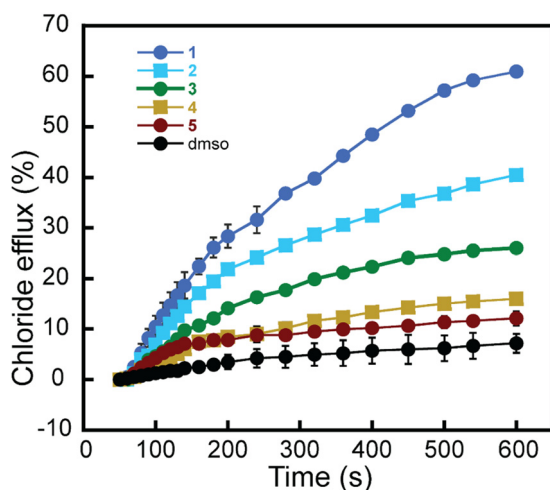
rates and the rates of membrane translocation for each anion. Perhaps the observed selectivity could be dictated by the rotaxane translocating chloride faster than other anions, as observed in other compounds participating in relay transport.<sup>54</sup>

Likewise, we also investigated if the type of the intravesicular cations influences the transport activity of rotaxane **1**. For this, different metal chlorides ( $\text{LiCl}$ ,  $\text{NaCl}$ ,  $\text{KCl}$ ,  $\text{RbCl}$ ,  $\text{CsCl}$ ) were



**Table 2** Transmembrane  $\text{Cl}^-$  transport efficiency of **1–5** at pH 7.2

Compound	$\text{EC}_{50}$ (mol%)
<b>1</b>	$0.243 \pm 0.080$
<b>2</b>	$0.736 \pm 0.109$
<b>3</b>	$4.044 \pm 0.280$
<b>4</b>	$4.986 \pm 0.810$
<b>5</b>	<sup>a</sup>

<sup>a</sup> Precipitation hinders the determination of its  $\text{EC}_{50}$  value.**Fig. 4** Transport of  $\text{Cl}^-$  anions across the bilayer of LUVs (EYPC/Chol, 8 : 2 molar ratio) by all the synthesized compounds at 0.499 mol%. The black curve corresponds to the sample where the DMSO stock solution was added to the LUVs without the rotaxane. Error bars represent standard deviations from two runs. Some error bars, though present, are so small that they are overshadowed by the symbols representing the data points.

separately encapsulated inside LUVs, whereas the external media consisted of a 5 mM phosphate buffer containing  $\text{NaNO}_3$ . We observed no significant changes in  $\text{Cl}^-$  transport among the different liposomes, thus ruling out any metal

dependency on the operation of the rotaxane (Fig. 5b and Fig. S29 and S30, ESI†).

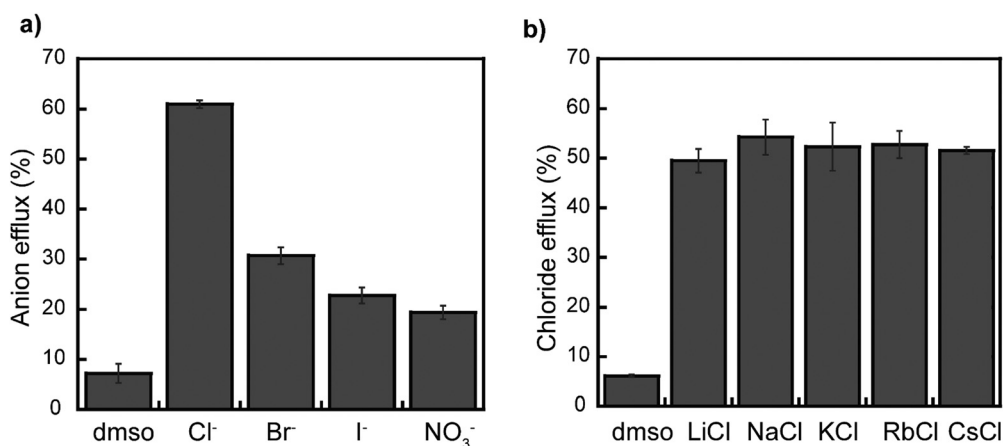
Furthermore, dynamic light scattering (DLS) measurements of the LUVs with and without rotaxanes **1–3** show similar average size distribution of the vesicles, indicating that incorporation of the rotaxanes does not cause their disassembly, as it is observed later upon addition of Triton X-100 (Fig. S31, ESI†). Likewise, leakage studies using the DPX-based quenching assay<sup>37</sup> revealed that incorporating the rotaxanes in the bilayer does not cause significant leakage from the vesicles (Fig. S32, ESI†).

Additionally, leaching tests were carried out to determine whether the rotaxanes remain solely in the membrane or if they diffuse to the aqueous phase. Using the ISE-based assay previously described, we evaluated the  $\text{Cl}^-$  efflux in samples featuring different concentrations of the vesicle solution (200, 300, 400, and 600  $\mu\text{M}$ ) while maintaining a constant rotaxane-to-lipid ratio. The rationale for this study is that if the rotaxanes leach from the membrane, the transport rate should decrease upon dilution as the equilibrium shifts.<sup>55,56</sup> However, similar transport rates were observed in all the samples, suggesting that rotaxane **1** predominately resides in the lipid membranes (Fig. S33 and S34, ESI†).

## 2.6 Antiport behavior of rotaxane 1

Having demonstrated that rotaxane **1** is an effective and selective transporter of  $\text{Cl}^-$  anions, we conducted a series of experiments to gather insights into its transport mechanism. Specifically, we sought to discern the most plausible process among  $\text{Cl}^-/\text{NO}_3^-$  antiport and  $\text{M}^+/\text{Cl}^-$  co-transport mechanisms based on the ISE-based transport assay.

First, we performed a classical U-tube experiment where the left arm was filled with  $\text{NaCl}$  solution, the right arm was filled with the  $\text{NaNO}_3$  buffer, and chloroform solution (organic phase) containing rotaxane **1** (0.2 mM) separated these two aqueous layers (Fig. 6a). In the presence of rotaxane **1**, the concentration of  $\text{Cl}^-$  anions increased in the right arm over

**Fig. 5** Anion and cation transport selectivity of rotaxane **1** in LUVs (EYPC/Chol, 8 : 2 molar ratio) at pH 7.2. (a)  $\text{X}^-$  anion efflux across LUVs encapsulating  $\text{NaX}$  ( $\text{X} = \text{Cl}^-, \text{Br}^-, \text{I}^-$  or  $\text{NO}_3^-$ ). (b)  $\text{Cl}^-$  anion efflux efficiency by rotaxane **1** across different LUVs encapsulating  $\text{MCl}$  ( $\text{M} = \text{Li}^+, \text{Na}^+, \text{K}^+, \text{Rb}^+$ , or  $\text{Cs}^+$ ). [**1**] = 0.499 mol% in both studies. DMSO bars correspond to the sample where the DMSO stock solution was added to the LUVs without rotaxane;  $\text{Cl}^-$  anions efflux was monitored for the DMSO samples. Error bars represent standard deviations from two runs.

100 h (green trace, Fig. 6c), whereas we did not observe any significant changes in the absence of the compound (red trace, Fig. 6c), which again demonstrates the  $\text{Cl}^-$  transport activity of rotaxane **1**. We suggest that  $\text{NO}_3^-$  anions are transported in the opposite direction than  $\text{Cl}^-$  anions, from the right arm to the left arm, to maintain charge neutrality, which implies a  $\text{Cl}^-/\text{NO}_3^-$  antiport process. It is important to mention that, in the U-tube, the rotaxane can transport the anions only by diffusion of the whole rotaxane-anion complex, and transport by shuttling is impossible in this setting because the rotaxanes are oriented randomly in the chloroform layer, which is several orders of magnitude larger than the lipid bilayer thickness. This experiment solely provides additional insights into the possibility of an antiport process. It is not intended to demonstrate/discard the transport by shuttling, relay, or diffusion in the lipid membrane.

Additionally, we conducted a reported fluorescence-based assay in which lucigenin and  $\text{NaNO}_3$  (200 mM) were encapsulated in the vesicles, while KCl (33 mM) and  $\text{NaNO}_3$  (200 mM) were present in the extravesicular media to establish a  $\text{Cl}^-/\text{NO}_3^-$  gradient.<sup>57</sup> Chloride transport by rotaxane **1** was evaluated in the presence and absence of valinomycin. A significant enhancement in the ion transport activity of rotaxane **1** was observed in the presence of valinomycin compared to rotaxane alone, confirming a  $\text{Cl}^-/\text{NO}_3^-$  antiport mechanism (Fig. S35, ESI†).

We carried out the classical U-tube assay to rule out the possibility of  $\text{H}^+/\text{Cl}^-$  co-transport. The left arm of the tube was filled with 0.1 N  $\text{HCl}_{\text{aq}}$  and the right arm was filled with isotonic  $\text{NaNO}_3$  solution (Fig. 6b). A chloroform solution (organic phase) containing rotaxane **1** (0.2 mM) separated these two aqueous solutions. The transport of  $\text{H}^+$  ions was directly recorded using a pH meter in the right arm over 100 h. In the presence of rotaxane **1**, changes in pH were comparable to those in the absence of rotaxane **1** (Fig. 6c). The pH decreases likely stems from minor solution diffusion between arms, suggesting that the rotaxane **1** did not significantly alter pH under the experimental conditions, ruling out the possibility of  $\text{H}^+/\text{Cl}^-$  co-transport (Fig. 6c).

Lastly, the metal dependency assay mentioned in the previous section (Fig. 5b) rules out interference of any metal ions during the transportation of  $\text{Cl}^-$  anions. As rotaxane **1** does not have any binding site available for metal ions, we assume there is no involvement of metals during the transport of  $\text{Cl}^-$  anions, ruling out the possibility of  $\text{M}^+/\text{Cl}^-$  co-transport.

## 2.7 Effect of membrane fluidity on anion transport

It is known that changes in membrane fluidity impact the function of transport proteins and synthetic ionophores.<sup>39,40</sup> Consequently, it is paramount to gain deeper insights into the effect of the membrane's composition and fluidity on the operation and transport activity of the rotaxanes.

Thus, we investigated the efficiency of rotaxanes **1** and **2** to transport  $\text{Cl}^-$  anions across lipid bilayers with different cholesterol content, which is known to increase membrane rigidity. We prepared LUVs with varying EYPC/Chol ratios (10:0, 8:2, and 6:4) and monitored the  $\text{Cl}^-$  anions efflux using the ISE-based assay. Notably, the highest transport activity for rotaxanes **1** and **2** was observed in the more fluid membrane with no cholesterol (Fig. 7b and c). As anticipated, increasing the cholesterol content (8:2 and 6:4) resulted in a reduction of  $\text{Cl}^-$  anion transport due to the increase in rigidity on the membranes, which decreased the freedom of movement required for potential shuttling and relay transport.

In a separate experiment, we investigated the  $\text{Cl}^-$  transport activity of the rotaxanes in bilayers composed of dipalmitoylphosphatidylcholine (DPPC), which has a phase transition temperature of 41 °C.<sup>58</sup> This means the membrane exists in the gel phase below 41 °C but transitions into a more fluid "liquid crystalline" phase at temperatures exceeding 41 °C. Both rotaxanes **1** and **2** showed negligible  $\text{Cl}^-$  anion transport at 25 °C when the bilayer is in the gel phase. However, at 45 °C, both rotaxanes recovered their transport capabilities in the fluid phase (Fig. 7d and e).

These experiments independently demonstrate that rotaxanes exhibit higher transport activity in membranes of higher fluidity. This could be attributed to both the ring shuttling

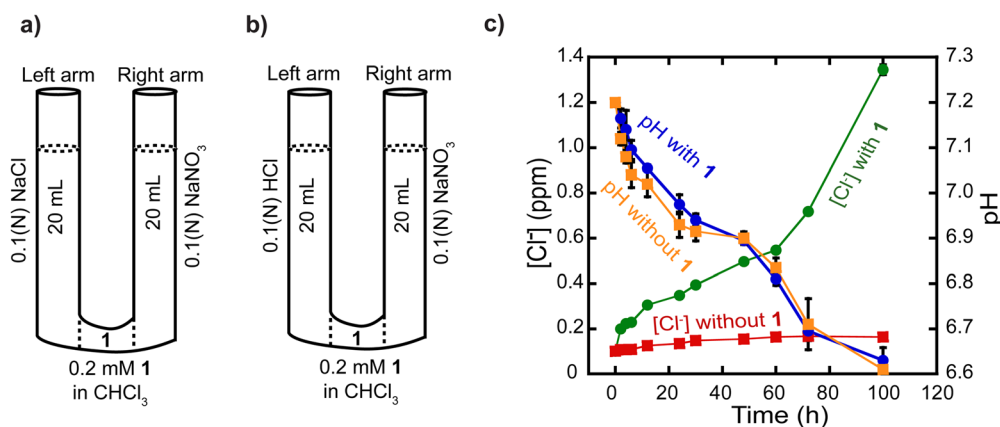


**Fig. 6** Transport of  $\text{Cl}^-$  anions across a U-tube. (a) and (b) Simple representation of the experimental setup. (c) Monitoring the  $\text{Cl}^-$  anions concentration and the pH over time using a pH meter and a  $\text{Cl}^-$  selective electrode, respectively. Error bars represent standard deviations from two runs. Some error bars, though present, are so small that they are overshadowed by the symbols representing the data points.





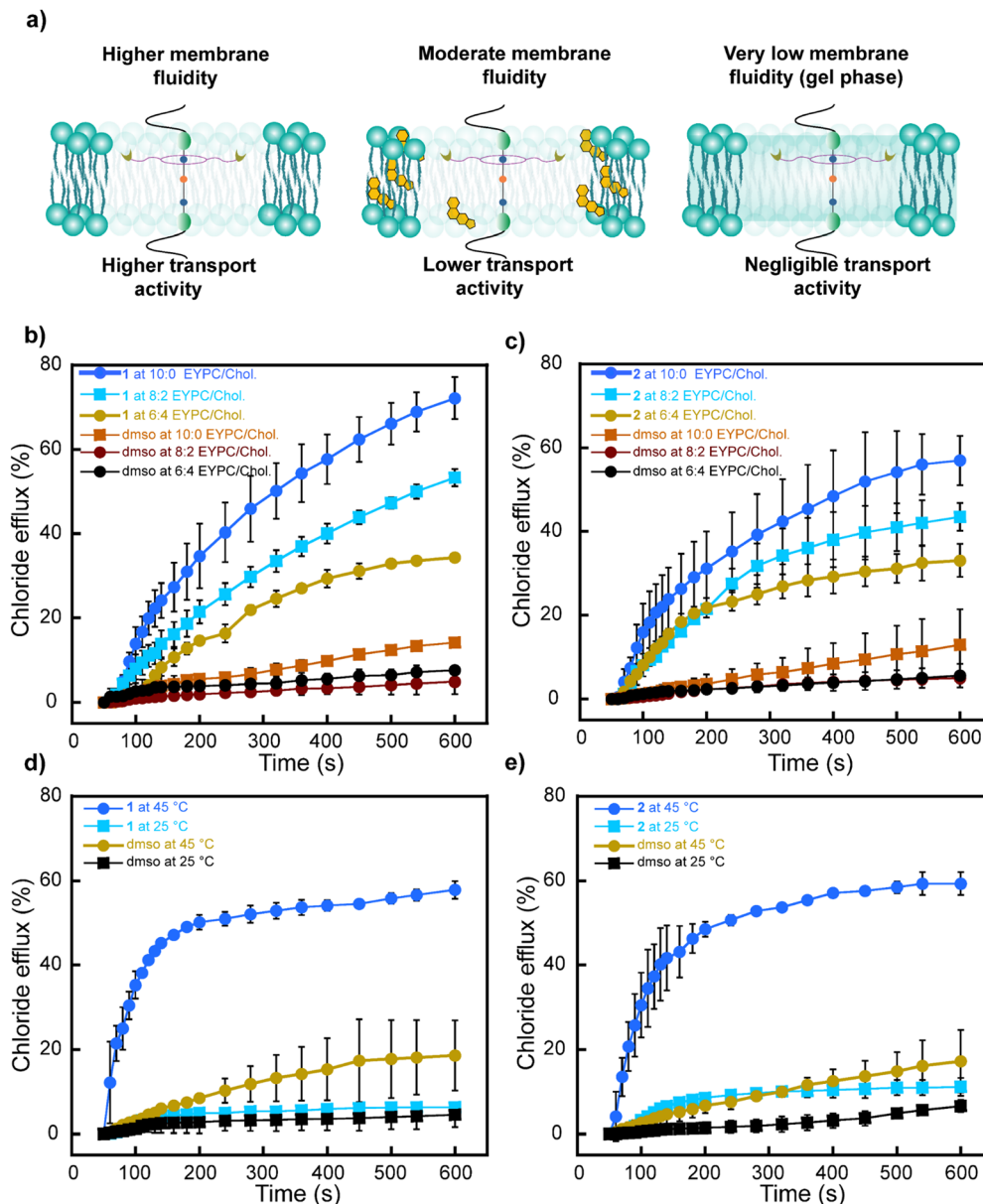


Fig. 7 Effect of membrane fluidity on anion transport. (a) Representation of the rotaxanes operation in membranes of different fluidity and composition. (b) and (c) Efficiency of rotaxanes **1** and **2** to transport  $\text{Cl}^-$  anions across EYPC membranes with different cholesterol content. (d) and (e) Efficiency of rotaxanes **1** and **2** to transport  $\text{Cl}^-$  anions across DPPC membranes below ( $25^\circ\text{C}$ ) and above ( $45^\circ\text{C}$ ) the phase transition temperature of the lipids. [**1**] = 0.499 mol%, [**2**] = 0.998 mol% in both studies. DMSO (dimethyl sulfoxide) curves correspond to the sample where the DMSO stock solution without the rotaxane was added to the LUVs. Error bars represent standard deviations from two runs. Some error bars, though present, are so small that they are overshadowed by the symbols representing data points.

more freely and a more favorable relay-based transport in such membrane environments.

### 2.8. Antibacterial activity against *Staphylococcus aureus*

Having demonstrated the efficiency of rotaxane **1** to transport  $\text{Cl}^-$  anions in synthetic lipid bilayers, we tested its ability to inhibit *S. aureus* growth through osmotic stress. *S. aureus* is osmotolerant, needing NaCl concentrations exceeding 2.5 M to completely inhibit growth without external anion transporters.<sup>25</sup> Thus, we treated *S. aureus* with 2  $\mu\text{M}$  rotaxane **1** and measured bacterial growth by optical density at 600 nm. As seen in Fig. 8a,

rotaxane **1** delays the visible growth of *S. aureus* by 8 h, which is a decrease in viable bacteria of 1.6 orders of magnitude or 46-fold over the first 4 h of the experiment (Fig. 8b). In this experiment, tryptic soy broth (TSB) has only 85 mM NaCl, so we hypothesized that this is not enough NaCl to overcome the osmotolerance of *S. aureus* even when cotreated with rotaxane **1**.

We then assessed the ability of rotaxane **1** to inhibit *S. aureus* growth in the presence of 1 M NaCl. NaCl at this concentration without rotaxane **1** slightly delayed *S. aureus* growth (Fig. 8a), resulting in a modest decrease in viable bacteria over the first 4 h (Fig. 8b), but *S. aureus* overcomes



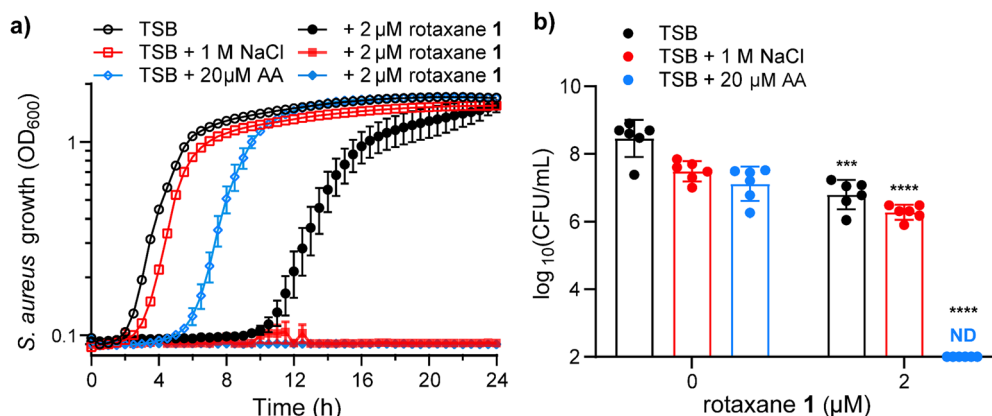


**Fig. 8** Rotaxane **1** kills *Staphylococcus aureus* by overcoming its inherent osmotolerance. (a) *S. aureus* growth was monitored by optical density at 600 nm for 24 h to determine the effects of rotaxane **1** in media with increased osmotic strength (1 M NaCl) or increased membrane fluidity (20 μM AA). Data presented are mean  $\pm$  S.E.M. acquired in sextuplet. (b) *S. aureus* viable colony forming units (CFU) were determined for the first 4 h of the kinetic growth curve by dilution plating under the same conditions. Data presented are mean  $\pm$  S.D. acquired in sextuplet. No colonies were detected in the TSB + 20 μM AA + 2 μM rotaxane **1**, so the data points were placed at the limit of detection for statistical analyses. Statistical significance was determined by an unpaired *t*-test where \*\*\* = *P* < 0.001 and \*\*\*\* = *P* < 0.0001.

this osmotic stress and reaches similar optical densities as the untreated strain by 8 h (Fig. 8a). Cotreatment of rotaxane **1** (2 μM) with 1 M NaCl shows no visible growth during the 24-hour kinetic growth curve (Fig. 8a). However, during the first 4 h, there is only a modest reduction in viable bacteria (Fig. 8b).

As we demonstrated in LUVs, rotaxane **1** transports ions more efficiently in more fluid membranes than rigid membranes. Therefore, we tested whether increasing the membrane fluidity in *S. aureus* would enhance the antibacterial properties of rotaxane **1**. We previously demonstrated that the fluidity of the membrane of *S. aureus* increases when polyunsaturated fatty acids, such as arachidonic acid (AA), are incorporated.<sup>21,41</sup> Arachidonic acid is an abundant polyunsaturated fatty acid with some toxicity against *S. aureus*.<sup>41</sup> Thus, treatment of *S. aureus* with 20 μM AA results in a 4 h delay in growth (Fig. 8a) and a modest decrease in viable bacteria (Fig. 8b). However, when *S. aureus* is cotreated with rotaxane **1** (2 μM) and AA (20 μM), there is no visible bacterial growth during the 24 h kinetic growth curve (Fig. 8a) and no viable bacteria 4 h post-treatment (Fig. 8b) in media containing only 85 mM NaCl. This remarkable result demonstrates that increased membrane fluidity exacerbates the ability of rotaxane **1** to kill *S. aureus*, even in conditions that do not have enough osmotic strength to affect *S. aureus* growth.

### 3 Conclusions

We report three new rotaxanes capable of transporting Cl<sup>−</sup> anions across synthetic lipid bilayers. Using molecules with distinctive molecular structures, we used different biophysical assays to identify the structural features and environmental conditions required for the rotaxanes' operation and anion transport activity in lipid membranes.

Structurally speaking, we validated that incorporating anion-recognition units on the ring of the rotaxane is an effective and promising way to transport Cl<sup>−</sup> across lipid membranes, as

showcased with rotaxanes **1** and **2**. On the contrary, rotaxane **3** without the thioureas showed significantly lower transport activity. Likewise, the axle (**4**) and ring (**5**) are also less efficient in transporting anions independently, proving the requirement of an interlocked molecule with anion recognition units.

Furthermore, we provide a deeper understanding of the intricate relationship between the rotaxanes and their anion transport efficacy. Thus, our findings demonstrate the ability to modulate transport activity by tuning the design of rotaxanes through structural changes and environmental conditions such as membrane fluidity and temperature. For instance, the higher transport efficiency of rotaxane **1**, compared to rotaxane **2**, could be tentatively correlated with its expedited ring shuttling. However, other transport mechanisms, such as relay transport, may contribute to the activity of the rotaxanes, too.

This study also demonstrates the antibacterial activity of rotaxane **1** against the drug-resistant pathogen *Staphylococcus aureus* when cotreated with either 1 M NaCl or 20 μM arachidonic acid in low NaCl concentration (85 mM). The antimicrobial activity of rotaxane **1** seems to correlate with its Cl<sup>−</sup> transport ability observed in liposomes; however, the mechanism to kill *S. aureus* may be more complex, and other factors could influence the observed antimicrobial activity of **1**. Still, this initial assessment opens the possibility of developing ion transporters based on rotaxanes in the future that can effectively inhibit *S. aureus* growth during food preservation without the need for overly salted foods, potentially broadening the range of healthier preserved foods. We envision further molecular optimization and mechanistic understanding, which will deliver rotaxanes with the potential to prevent nosocomial infections. Two-thirds of the human population will be colonized with *S. aureus* at some point in their life,<sup>59</sup> and the colonizing *S. aureus* strain is typically the causative agent of invasive infections for these patients, making decolonization an important step prior to many medical procedures.<sup>59</sup> Additionally, bacteria regularly grow on hospital surfaces and



can become the seeds for future nosocomial infections.<sup>60</sup> The data we present here suggest hospital surface decontamination could be achieved in the future by combining advanced rotaxanes that transport Cl<sup>−</sup> with saline (154 mM NaCl) as a cleaning solution.

## Author contributions

N. A. measured the binding constants, conducted anion transport studies in liposomes, and completed the last steps of the synthesis. U. N. K. C. carried out most of the synthesis. S. P. B. performed the bacterial studies under the supervision of W. N. B. Z. A. A. conducted the fluorescence assays. M. L. D. synthesized important precursors early in the project. N. A., W. N. B., and V. G. L. wrote the manuscript, and all the authors contributed to the proofreading and editing. W. N. B. secured funding and designed bacterial experiments. V. G. L. secured funding and conceived and supervised the project.

## Data availability

The data supporting this article have been included as part of the ESI.†

## Conflicts of interest

The authors declare no conflict of interest.

## Acknowledgements

V. G. L. holds a Career Award at the Scientific Interface from Burroughs Wellcome Fund. W. N. B. is supported by an NIAID Career Transition Award (K22AI153677) and LSU SVM startup funds. S. P. B. is supported through a D. V. M. Summer Scholars Research Grant from Boehringer Ingelheim and the LSU SVM. We thank Prof. Mathew Chambers for providing access to their fluorometer.

## References

- 1 N. Akhtar, O. Biswas and D. Manna, *Chem. Commun.*, 2020, **56**, 14137–14153.
- 2 L. Imholt, D. Dong, D. Bedrov, I. Cekic-Laskovic, M. Winter and G. Brunklaus, *ACS Macro Lett.*, 2018, **7**, 881–885.
- 3 C. Tang and M. L. Bruening, *J. Polym. Sci.*, 2020, **58**, 2831–2856.
- 4 Y. Garba, S. Taha, N. Gondrexon and G. Dorange, *J. Membr. Sci.*, 1999, **160**, 187–200.
- 5 R. Tan, A. Wang, R. Malpass-Evans, R. Williams, E. W. Zhao, T. Liu, C. Ye, X. Zhou, B. P. Darwich and Z. Fan, *Nat. Mater.*, 2020, **19**, 195–202.
- 6 W. Xin, L. Jiang and L. Wen, *Angew. Chem., Int. Ed.*, 2022, **134**, e202207369.
- 7 J. Yang, G. Yu, J. L. Sessler, I. Shin, P. A. Gale and F. Huang, *Chem.*, 2021, **7**, 3256–3291.
- 8 J. T. Davis, P. A. Gale and R. Quesada, *Chem. Soc. Rev.*, 2020, **49**, 6056–6086.
- 9 A. Roy and P. Talukdar, *ChemBioChem*, 2021, **22**, 2925–2940.
- 10 U. Bukovnik, M. Sala-Rabanal, C. Nichols, B. Schultz, J. Chen and J. Tomich, *Biophys. J.*, 2011, **100**, 87a.
- 11 T. Saha, M. S. Hossain, D. Saha, M. Lahiri and P. Talukdar, *J. Am. Chem. Soc.*, 2016, **138**, 7558–7567.
- 12 T. Saha, A. Gautam, A. Mukherjee, M. Lahiri and P. Talukdar, *J. Am. Chem. Soc.*, 2016, **138**, 16443–16451.
- 13 N. Akhtar, N. Pradhan, G. K. Barik, S. Chatterjee, S. Ghosh, A. Saha, P. Satpati, A. Bhattacharyya, M. K. Santra and D. Manna, *ACS Appl. Mater. Interfaces*, 2020, **12**, 25521–25533.
- 14 N. Busschaert, S.-H. Park, K.-H. Baek, Y. P. Choi, J. Park, E. N. Howe, J. R. Hiscock, L. E. Karagiannidis, I. Marques and V. Félix, *Nat. Chem.*, 2017, **9**, 667–675.
- 15 S. Dey, A. Patel, N. Haloi, S. Srimayee, S. Paul, G. K. Barik, N. Akhtar, D. Shaw, G. Hazarika and B. M. Prusty, *J. Med. Chem.*, 2023, **66**, 11078–11093.
- 16 A. I. Share, K. Patel, C. Nativi, E. J. Cho, O. Francesconi, N. Busschaert, P. A. Gale, S. Roelens and J. L. Sessler, *Chem. Commun.*, 2016, **52**, 7560–7563.
- 17 C. R. Elie, G. David and A. R. Schmitzer, *J. Med. Chem.*, 2015, **58**, 2358–2366.
- 18 I. Carreira-Barral, C. Rumbo, M. Mielczarek, D. Alonso-Carrillo, E. Herran, M. Pastor, A. Del Pozo, M. García-Valverde and R. Quesada, *Chem. Commun.*, 2019, **55**, 10080–10083.
- 19 M. B. Patel, E. C. Garrad, A. Stavri, M. R. Gokel, S. Negin, J. W. Meisel, Z. Cusumano and G. W. Gokel, *Bioorg. Med. Chem.*, 2016, **24**, 2864–2870.
- 20 A. L. Santos, A. van Venrooy, A. K. Reed, A. M. Wyderka, V. García-López, L. B. Alemany, A. Oliver, G. P. Tegos and J. M. Tour, *Adv. Sci.*, 2022, **9**, 2203242.
- 21 W. N. Beavers, M. J. Munneke, A. R. Stackhouse, J. A. Freiberg and E. P. Skaar, *Microbiol. Spectrum*, 2022, **10**, e02767–02721.
- 22 P. L. Graham, 3rd, S. X. Lin and E. L. Larson, *Ann. Intern. Med.*, 2006, **144**, 318–325.
- 23 S. Y. Tong, J. S. Davis, E. Eichenberger, T. L. Holland and V. G. Fowler Jr, *Clin. Microbiol. Rev.*, 2015, **28**, 603–661.
- 24 C. Antimicrobial Resistance, *Lancet*, 2022, **399**, 629–655.
- 25 Y. Feng, T. Ming, J. Zhou, C. Lu, R. Wang and X. Su, *Foods*, 2022, **11**, 1503.
- 26 W.-Z. Wang, L.-B. Huang, S.-P. Zheng, E. Moulin, O. Gavet, M. Barboiu and N. Giuseppone, *J. Am. Chem. Soc.*, 2021, **143**, 15653–15660.
- 27 V. García-López, F. Chen, L. G. Nilewski, G. Duret, A. Aliyan, A. B. Kolomeisky, J. T. Robinson, G. Wang, R. Pal and J. M. Tour, *Nature*, 2017, **548**, 567–572.
- 28 T. G. Johnson and M. J. Langton, *J. Am. Chem. Soc.*, 2023, **145**, 27167–27184.
- 29 J. P. Sauvage, *Angew. Chem., Int. Ed.*, 2017, **56**, 11080–11093.
- 30 I. Aprahamian, *ACS Cent. Sci.*, 2020, **6**, 347–358.
- 31 Y. Feng, M. Ovalle, J. S. Seale, C. K. Lee, D. J. Kim, R. D. Astumian and J. F. Stoddart, *J. Am. Chem. Soc.*, 2021, **143**, 5569–5591.



- 32 V. García-López, D. Liu and J. M. Tour, *Chem. Rev.*, 2019, **120**, 79–124.
- 33 A. Mondal, M. Ahmad, D. Mondal and P. Talukdar, *Chem. Commun.*, 2023, **59**, 1917–1938.
- 34 S. Chen, Y. Wang, T. Nie, C. Bao, C. Wang, T. Xu, Q. Lin, D.-H. Qu, X. Gong and Y. Yang, *J. Am. Chem. Soc.*, 2018, **140**, 17992–17998.
- 35 C. Wang, S. Wang, H. Yang, Y. Xiang, X. Wang, C. Bao, L. Zhu, H. Tian and D. H. Qu, *Angew. Chem., Int. Ed.*, 2021, **133**, 14962–14966.
- 36 H. Zhang, Y. Guo, C. Chipot, W. Cai and X. Shao, *J. Phys. Chem. Lett.*, 2021, **12**, 3281–3287.
- 37 S. Pang, X. Sun, Z. Yan, C. Wang, K. Ye, S. Ma, L. Zhu and C. Bao, *Chem. Commun.*, 2023, **59**, 3866–3869.
- 38 K. Ye, Z. Zhang, Z. Yan, S. Pang, H. Yang, X. Sun, C. Liu, L. Zhu, C. Lian and C. Bao, *Sci. China: Chem.*, 2023, **66**, 2300–2308.
- 39 V. Bolotina, V. Omelyanenko, B. Heyes, U. Ryan and P. Bregestovski, *Pfluegers Arch.*, 1989, **415**, 262–268.
- 40 E. Lyman, *Biophys. J.*, 2021, **120**, 193a.
- 41 W. N. Beavers, A. J. Monteith, V. Amarnath, R. L. Mernaugh, L. J. Roberts, W. J. Chazin, S. S. Davies and E. P. Skaar, *mBio*, 2019, **10**(5), e01333-19.
- 42 S. Chao, C. Romuald, K. Fournel-Marotte, C. Clavel and F. Coutrot, *Angew. Chem., Int. Ed.*, 2014, **53**, 6914–6919.
- 43 F. Coutrot and E. Busseron, *Chem. – Eur. J.*, 2008, **14**, 4784–4787.
- 44 P. Waelès, C. Clavel, K. Fournel-Marotte and F. Coutrot, *Chem. Sci.*, 2015, **6**, 4828–4836.
- 45 O. Š. Miljanić, W. R. Dichtel, I. Aprahamian, R. D. Rohde, H. D. Agnew, J. R. Heath and J. Fraser Stoddart, *QSAR Comb. Sci.*, 2007, **26**, 1165–1174.
- 46 I. Smukste, B. E. House and D. B. Smithrud, *J. Org. Chem.*, 2003, **68**, 2559–2571.
- 47 I. Smukste and D. B. Smithrud, *J. Org. Chem.*, 2003, **68**, 2547–2558.
- 48 C. J. Bruns and J. F. Stoddart, *The nature of the mechanical bond: from molecules to machines*, Wiley, 2016.
- 49 P. Thordarson, *Chem. Soc. Rev.*, 2011, **40**, 1305–1323.
- 50 D. B. Hibbert and P. Thordarson, *Chem. Commun.*, 2016, **52**, 12792–12805.
- 51 N. Akhtar, O. Biswas and D. Manna, *Org. Biomol. Chem.*, 2021, **19**, 7446–7459.
- 52 X. Wu and P. A. Gale, *Chem. Commun.*, 2021, **57**, 3979–3982.
- 53 A. M. Gilchrist, P. Wang, I. Carreira-Barral, D. Alonso-Carrillo, X. Wu, R. Quesada and P. A. Gale, *Supramol. Chem.*, 2021, **33**, 325–344.
- 54 T. G. Johnson, A. Docker, A. Sadeghi-Kelishadi and M. J. Langton, *Chem. Sci.*, 2023, **14**, 5006–5013.
- 55 N. Akhtar, A. Saha, V. Kumar, N. Pradhan, S. Panda, S. Morla, S. Kumar and D. Manna, *ACS Appl. Mater. Interfaces*, 2018, **10**, 33803–33813.
- 56 M. Lisbjerg, H. Valkenier, B. M. Jessen, H. Al-Kerdi, A. P. Davis and M. Pittelkow, *J. Am. Chem. Soc.*, 2015, **137**, 4948–4951.
- 57 J. A. Malla, R. M. Umesh, A. Vijay, A. Mukherjee, M. Lahiri and P. Talukdar, *Chem. Sci.*, 2020, **11**, 2420–2428.
- 58 H. Behera and N. Madhavan, *J. Am. Chem. Soc.*, 2017, **139**, 12919–12922.
- 59 P. L. Graham III, S. X. Lin and E. L. Larson, *Ann. Intern. Med.*, 2006, **144**, 318–325.
- 60 S. J. Dancer, *Clin. Microbiol. Rev.*, 2014, **27**, 665–690.

